Supporting Information

Optomechanical and crystallization phenomena visualized with 4D electron microscopy: Interfacial carbon nanotubes on silicon nitride

David J. Flannigan[1] and Ahmed H. Zewail[1*]

[1]Physical Biology Center for Ultrafast Science and Technology, Arthur Amos Noyes Laboratory of Chemical Physics, California Institute of Technology, Pasadena, CA, 91125 USA.

[*]email: zewail@caltech.edu

Methods

UEM Methodology. While the UEM methodology can be adjusted to suit many different experimental parameters, only the specific configuration used here will be described; overviews of the concept of UEM and apparatus are detailed elsewhere for the interested reader.[1-4] Recall that traditional transmission electron microscopes (TEMs) are operated using a continuous electron beam generated by thermionic emission and/or high-field extraction. That is, the arrival of electrons at the specimen is random in time. Time-resolved studies must therefore be conducted with fast CCD cameras, which currently can provide tens of milliseconds temporal resolution.[5] Unlike traditional microscopes, UEM can be operated in a pulsed mode; discrete packets of single electrons are photoelectrically generated by illuminating the microscope cathode (e.g., LaB_6) with femtosecond optical laser pulses. Another femtosecond laser beam is used to excite the sample *in situ*. Time-resolved studies are conducted using a pump/probe stroboscopic methodology, which is achieved by varying the arrival time of the excitation laser pulse at the sample relative to that of the discrete photoelectron packet. For the work reported here, 120 fs pulses (776 nm), generated at a repetition rate of 80 MHz and frequency doubled to 388 nm, were used to generate the discrete photoelectron packets. The time delay is achieved by using an optical translation stage to change the arrival time of the excitation laser pulse at the sample relative to the electron packets. By operating below the regime where space-charge is the limiting factor[2,4] – the single-electron regime – spatial resolutions comparable to those of standard electron microscopes can be achieved,[1,3] but with ultrafast temporal resolution. The stroboscopic methodology means that each image generated is comprised of many pulses, the total number of which is the product of the laser repetition rate and acquisition time. Here, all images were acquired in 15 seconds, thus each image is built up from 1.2×10^9 pulses. Once an

image is acquired at a specific point in time, the optical translation stage is moved to a new position and the next image is acquired. We note that UEM can also be operated as a traditional TEM, but with the added capability of *in situ* laser heating of specimens,[6,7] as was done for the Si_3N_4 crystallization observations reported here.

Specimen Preparation and *in situ* Excitation. The amorphous Si_3N_4 mesh (Ted Pella, Inc.) consisted of 7 μm holes pitched at 9 μm and was 200 nm thick. While the stoichiometry of the mesh may not be exactly Si_3N_4 due to oxygen contamination and other factors, the precise ratio of elements in no way affects the interpretation of our observations. The MSDS for Si_3N_4 mesh grids provided by Ted Pella, Inc. list the entire grid composition as 0.025 wt% SiN, 0.025 wt% SiO_2, and 99.95wt% Si.[8] The 99.95 wt% Si refers to the silicon substrate upon which the SiN film is grown and not to the silicon content in the film itself. All grids provided by Ted Pella, Inc. list the silicon nitride stoichiometry as Si_3N_4. The mesh window measured 500 x 500 μm square and was atop a 300 μm thick silicon substrate that was 3 x 3 mm. The multiwalled carbon nanotubes (CNTs; 1.9 mg, Aldrich, >90% purity, 0.1 to 10 μm in length) were dispersed in 5.1 mL of nanopure water (18 MΩ·cm) containing sodium dodecyl sulfate (SDS; 16.7 mg, Aldrich, 99+% purity) via sonication for 18 hr. After sonication, the mixture was spun in a centrifuge (6,000 rpm for 30 minutes), and the top layer was decanted and separated from the denser portion, which was discarded. A droplet of the decanted mixture was placed onto the Si_3N_4 mesh, and the entire specimen was placed into a tube furnace at 80 °C with a flow of dry argon for 30 min. After cooling, the specimen was gently rinsed with nanopure water and placed back into the furnace for 1 hr.

There are two distinct observations we report here. The first is the *in situ* crystallization of the amorphous Si_3N_4 mesh, which is mediated by the adhering CNT network. The second is

the ultrafast optomechanical motion of the specimen. The crystallization is performed by operating UEM in a continuous mode with *in situ* laser heating capabilities. While observing the sample, a train of femtosecond laser pulses (80 MHz, 776 nm, 10 mW, 50 μm spot size FWHM) were admitted into the microscope with a mechanical shutter. The crystallization occurred much faster than could be resolved with the real-time display of the microscope (< 0.5 seconds). It is important to realize that this crystallization is separate from and occurs prior to any stroboscopic time-resolved studies; the crystallization of Si_3N_4 and thermal expansion of the CNT intertubule spacings shown in Figure 2 of the main Text arise from photothermal heating of the specimen by illumination with the laser pulses. The time-resolved studies of the optomechanical motion of the specimen are performed by operating UEM in pump/probe stroboscopic mode. This means that the ultrafast motion shown in Figures 3, 4, and 5 is due to a single 120 fs excitation laser pulse (776 nm, 6.4 $\mu J/cm^2$). The experiments can be conducted stroboscopically at 80 MHz.

Diffraction Calibration of UEM. The calibration procedure of UEM for absolute diffraction pattern measurements used here is similar to that for standard TEMs. That is, a diffraction pattern of a standard sample (evaporated Al film; Ted Pella, Inc.) was acquired with all the same lens currents, high voltage settings, and in the same stage position (or as close as possible) as were used for the unknown (i.e., CNT network). The only major addition to this for UEM is that the laser settings (i.e., position, power, wavelength, stability, etc.) used to generate the photoelectron packets must be the same for the standard as that used for the unknown. Once a diffraction pattern of the standard Al film was acquired and the indices assigned to the known *d* spacings, the diameter of each ring, *S*, was determined. Then, a constant, *K*, which represents the average electron beam wavelength, camera length, and variable crystallographic data, was determined by taking the average of the product of *d* and *S* for each visible diffraction ring. This

constant was then applied to the diffraction pattern of the unknown in order to determine the absolute *d* spacings and assign the crystallographic planes producing the observed rings. It is important to do absolute calibrations when switching between UEM and TEM modes, as the radii of diffraction rings can differ by a few tenths of a percent due to changes in effective source size and position, as well as beam convergence/divergence. This procedure is less critical when studying relative changes only.

Calibration of Diffraction Contrast Motion with an Image Tilt Series. To calibrate the diffraction contrast motion shown in Fig. 5 of the main Text, the direction of deflection must be known and properly reproduced in a standard TEM tilt series of images. This means that the effective specimen tilt axis for the time-resolved images must be carefully determined. To find the quasi steady-state position, a time-averaged (i.e., continuous electron beam) image of the specimen exposed to the train of femtosecond laser pulses is obtained. This image is then cross-correlated with images of the specimen obtained at various tilt angles and positions when not exposed to the pulse train until a coefficient as close to one as possible is reached. Once the position is established, a particular diffraction contrast feature is selected, and the motion as a function of time is quantified; in Fig. 5, the motion is relative to the contrast feature position at time zero. The position of the diffraction contrast feature shown in Fig. 5a is determined by fitting its profile with a symmetric peak function to find the center; the orange dashed line marks the peak center position. To determine the amount and direction of specimen tilting which gives rise to the observed diffraction contrast motion, the motion of the same feature is measured as a function of sample stage tilt angle. Here, the feature position was measured at 0.1 degree intervals, and a calibration curve was established (Fig. 5a plot). In this way, both the direction of

laser-induced deflection and the degree of deflection in degrees as a function of time can be determined.

Drift Correction and Dynamics Quantification. In order to isolate the true dynamics of the system from sample drift, a rapid toggling technique was used to analyze images post experiment. That is, drift is not automatically corrected during the experiment; no manual or automated specimen shifting is done during the experiment. The toggling technique makes use of visual sensitivity to minor differences in images that are layered and then quickly switched between. For a UEM time scan, each image within the series is quickly toggled back and forth with a reference image, which is also part of the series (e.g., first frame acquired in the scan). The image is then manually shifted with one pixel resolution relative to the reference image until the effect of specimen drift is minimized. During the manual drift correction, each image within the UEM time scan is linearly scaled from 0 to 255. It is important to note that we made use of the curved edge of the Si_3N_4 mesh for post experiment drift correction; we did not use any regions showing diffraction contrast due to the inherent complexity involved with that process. In this way, the physical position of the specimen was easily fixed in space by drift correction without suffering from the added complexity of diffraction contrast dynamics. The curved edge of the Si_3N_4 mesh to which we refer can be clearly seen on the left side of Fig. 3c of the main Text. For the work reported here, the maximum drift observed for all experiments was 21 pixels for a 1,024 x 1,024 pixel image. At the magnification used for this experiment, this translates to just over a 39 nm drift. Taking into account the experiment duration [here, it is: (15 second acquisition + 5 second readout time) * 135 images = 2700 seconds experiment time], this corresponds to a drift rate of about 0.9 nm per minute. Note that this exceeds the specifications for drift rate for our machine during installation (2 nm per minute). We are able to achieve this

level of stability by allowing the apparatus to thoroughly stabilize. Prior to conducting any time-resolved experiments, the UEM apparatus is allowed to stabilize at the desired settings, and the sample is irradiated with the excitation laser pulses overnight in order to minimize drift due to thermal gradients. Once stability is verified by measuring electron beam intensity and position as a function of time and specimen drift rate, the time-resolved experiments are conducted. The same level of stability is also applied to all controls.

Once the drift is isolated and corrected for post experiment, the relative changes in diffraction contrast of the crystalline Si_3N_4 are quantified using a series of simple mathematical operations similar to how a traditional cross correlation is conducted. The process used here makes use of a series of simple mathematical operations applied to each UEM image in relation to a reference image. The reference image was the first image acquired in the scan. Each image in the scan is subtracted from the reference image, and the result is squared and summed. Dividing the sum of a reference image by all other sums for each time step provides an image correlation coefficient, where 1 denotes a perfect correlation (i.e., no change) and 0 denotes no correlation. Note that this method produces the exact same temporal responses as any other method used (e.g., cross correlation, difference image summing, etc.). That is, the dynamics do not depend upon the specific data analysis technique used.

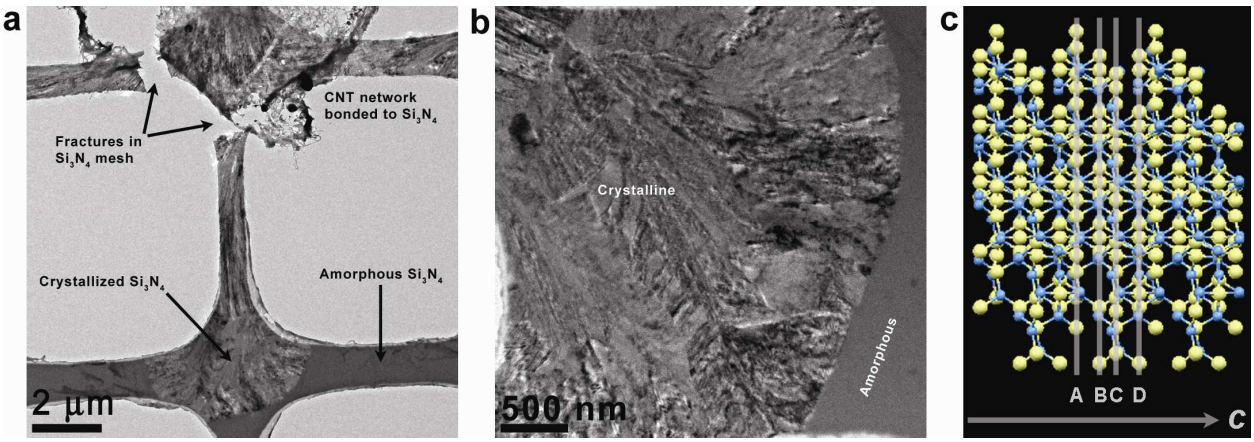

Supporting Figure 1. Overview of the Si_3N_4 mesh after the laser-induced amorphous-to-crystalline phase transition. **a,** Low-magnification (1,650x) image of the Si_3N_4 mesh with the adhering CNT network (top of image). The lower section of the mesh that has fractured and separated from the upper section with the CNT network shows both crystalline and amorphous regions. The lower section is devoid of CNTs, as was determined by careful inspection. The fractures of the mesh occurred during the phase transition. **b,** Higher-magnification (6,500x) image of the Si_3N_4 mesh showing both crystalline and amorphous regions (labeled as such in the Figure). This section is also devoid of CNTs. **c,** Crystal structure of α-Si_3N_4 viewed perpendicular to the crystallographic *c*-axis. The ABCD stacking arrangement is shown with the planes highlighted. Silicon is shown in yellow, while nitrogen is in blue.

Supporting Movie 1. 181 frames at 10 fps. Movie of a tilt series of images of the crystalline Si_3N_4 mesh with adhering CNT network. The range of tilting was from -45.0 to +45.0 degree, with steps of 0.5 degree. The tilt angle at which each image was acquired is shown in the upper left corner of each frame. Zero degree denotes the angle at which the sample is perpendicular to the incoming electron packets. Negative angles correspond to sample stage rotations that are counterclockwise from zero, while positive angles are clockwise. For reference, the handle of the sample holder is toward the bottom of the image. Thus, the movie begins with the left-side of the sample, as viewed in the images, tilted away from the viewer. As the angles become more positive, the sample tilts from left to right. At +45.0 degree, the right-side of the sample is now tilted away from the viewer. The apparent shimmering of the Si_3N_4 mesh is due to the change in diffraction contrast with tilt angle, as discussed in the text.

Supporting Movie 2. 20 frames at 2 fps. Movie of a region of Si_3N_4 with adhering CNT network showing macroscopic optomechanical motion. The sample was actuated with a train of fs laser pulses, which were either blocked (laser blocked) or unblocked (laser unblocked) with a mechanical shutter. The images were obtained at a magnification of 3,200x in standard TEM mode (i.e., with a continuous electron beam).

Supporting Movie 3. 20 frames at 2 fps. Movie of a bundle of CNTs adhering to the Si_3N_4 mesh showing nanoscopic optomechanical motion. The sample was actuated with a train of fs laser pulses, which were either blocked (laser blocked) or unblocked

(laser unblocked) with a mechanical shutter. The images were obtained at a magnification of 6,500x in standard TEM mode (i.e., with a continuous electron beam).

Supporting Movie 4. 132 frames at 10 fps. Movie of the picosecond temporal dependence of the Si_3N_4 diffraction contrast. The frames are difference images obtained by subtracting an image obtained at time *t*, where *t* is one of the 132 frames that range from -325 to +985 ps at 10 ps steps, from a reference image obtained at -335 ps. The movie shows the real-time dynamics of the Si_3N_4 slowed by a factor of 10^7. The time relative to time zero to which each frame corresponds is shown in the upper right corner. Each image was obtained at a magnification of 11,000x. The apparent minor changes before time zero are caused by minor systematic variations that are minimized via the rigorous controls detailed above. Note that the difference contrast pattern shown in the movie is opposite from that shown in Fig. 4 of the main text simply because the order of subtraction was different. This in no way changes any results or interpretation thereof.

References

1. Barwick, B.; Park, H. S.; Kwon, O. H.; Baskin, J. S.; Zewail, A. H. *Science* **2008**, *322*, 1227.

2. Lobastov, V. A.; Srinivasan, R.; Zewail, A. H. *Proc. Natl. Acad. Sci. U.S.A.* **2005**, *102*, 7069.

3. Park, H. S.; Baskin, J. S.; Kwon, O. H.; Zewail, A. H. *Nano Lett.* **2007**, *7*, 2545.

4. Zewail, A. H.; Thomas, J. M., *4D Electron Microscopy: Imaging in Space and Time*. Imperial College Press: London, 2009.

5. Tsung, L.; Mollon, B.; Jia, Y.; Mooney, P.; Mao, C.; Pan, M. *Microsc. Microanal.* **2008**, *14*, 808.

6. Flannigan, D. J.; Lobastov, V. A.; Zewail, A. H. *Angew. Chem., Int. Ed. Engl.* **2007**, *46*, 9206.

7. Taheri, M. L.; Lagrange, T.; Reed, B. W.; Armstrong, M. R.; Campbell, G. H.; DeHope, W. J.; Kim, J. S.; King, W. E.; Masiel, D. J.; Browning, N. D. *Microsc. Res. Techniq.* **2009**, *72*, 122.

8. http://www.tedpella.com/msds_html/21500-10_to_21525-100_21535_21540-10_to_21542-10_21555_MSDS.pdf